Journal of Asian Ceramic Societies 5 (2017) 391–396

Contents lists available at ScienceDirect

Journal of Asian Ceramic Societies

journal homepage: www.elsevier.com/locate/jascer

Role of cobalt doping on the electrical conductivity of ZnO nanoparticles

Umadevi Godavarti[a,c], V.D. Mote[b], Madhavaprasad Dasari[c,*]

[a] Department of Physics, CMR Technical Campus, Medchel, Hyderabad, 501 401, Telangana, India
[b] Thin Films and Materials Research Laboratory, Department of Physics, Dayanand Science College, Latur, 413 512, Maharashtra, India
[c] Department of Physics, GITAM Institute of Technology, GITAM University, Visakhapatnam, 530045, Andhra Pradesh, India

ARTICLE INFO

Article history:
Received 4 May 2017
Received in revised form 19 July 2017
Accepted 11 August 2017
Available online 22 August 2017

Keywords:
Chemical synthesis
ZnO nanoparticles
XRD
Spherical structure
Electrical conductivity

ABSTRACT

Cobalt doped zinc oxide ($Zn_{1-x}Co_xO$; x = 0, 0.05, 0.10, 0.15) samples were synthesized using co-precipitation method. The Co doped ZnO nanoparticles showed the maximum solubility limit. The XRD patterns confirm the hexagonal type wurtzite structure without secondary phase in Co substituted ZnO samples. The particle size was studied using transmission electron microscope (TEM) and grain size estimated using scanning electron microscope (SEM). We report the study of temperature dependence of conductivity on ZnO and Co doped ZnO nanoparticles. It is found that at a higher temperature range (above 470 K) thermally activated type of conduction is in dominance with the lower temperature range of conduction in which donor carrier hopping mechanism is dominated. DC conductivity result shows the reduction nature for cobalt doped ZnO. The obtained results are discussed on basis of potential barrier, donor concentration, point defects and adsorption–desorption of oxygen. Cobalt substitution increases resistivity, reduces grain growth, lower particle size and increase in activation energy. Detailed mapping of two regions of electrical conductivity is done to understand the activation energy mechanisms prevailing in cobalt doped ZnO.

1. Introduction

Zinc oxide (ZnO) is a II–VI group semiconductor has a wurtzite crystal structure, with a direct and wide bandgap of 3.37 eV, a large exciton binding energy (60 meV) and high optical gain at room temperature [1–3]. Numerous applications of wurtzite ZnO comprises of field-effect transistor [4], optical device [5], dye-sensitized solar cell [6], solid-state gas sensor [7,8]. The strong n-type conductivity is exhibited by zinc oxide varistor (ZnO) with the electrons to move in the conduction band as charge carriers. Primary dependence of electrical properties of ZnO is based on the composition and on microstructure characteristics such as grain size, density and morphology. The study of effect of dopants on physical and electrical properties of ZnO are related to applications in electronic components such as piezoelectric transducers and varistor.

Most of the ZnO nanomaterials have been fabricated by conventional high temperature solid state mechanisms which is energy consuming and unfavorable to control the particle properties [9]. ZnO nanoparticles can be synthesized by simple solution based methods on a large scale such as chemical precipitation, sol–gel synthesis, and solvothermal/hydrothermal reaction [10]. We synthesized ZnO nano powders using precipitation method at a sintering temperature of 400 °C. This fabrication method has been successfully employed in our work to prepare nanoscale particles being cost-effective and controlled which desires low temperatures for processing and a high degree of solubility can be acquired.

Among many research dopants in zinc oxide, cobalt doped zinc oxide shows potential in various applications [11,12]. According to reference studies [13], doping Cobalt in ZnO creates more zinc vacancies. Thus among diluted magnetic semiconductors (DMS), Cobalt doped ZnO is considered as a potential candidate among the TM because of its abundant electron states, large solubility in the ZnO matrix and also cobalt has a similar ionic radius (0.58 Å) to that of Zn (0.60 Å) [14]. Further different complex morphologies such as flowers, rods, sheets etc require too many control parameters which limit the application of the nanostructures.

The presence of secondary phases like Co^{3+} ions which may coexist with Co^{2+} ions in Co doped ZnO nanoparticles, are expected to have lattice defects [15]. Kumar and Khare, Roy et al. [16,17] and Yan et al. [18] reported increase in resistivity of Co^{2+} doped

* Corresponding author.
E-mail address: madhavaprasaddasari@gmail.com (M. Dasari).

http://dx.doi.org/10.1016/j.jascer.2017.08.002

ZnO samples, can be attributed to the shallow acceptor nature of these impurities. Birajdar et al. [19] and Kulandaisamy et al. [20] reported an increase in resistivity due to cobalt defect scattering centre in the ZnO lattice. Substitution of any dopant can expect changes in lattice parameter (a,c) and volume (V) showing initial proof of doping effects. Creating defects or doping in zinc oxide to generate multi-valence nature in the system to tailor the level or occupancy of the fermi energy level further affects the conductivity nature [21]. Doping any element in zinc oxide could produce distortions, results variations in optical band gap [22]. Considering the Burtein-Moss effect, the band gap value increases with the number of carrier concentration in conduction band. This could be also verified using conductivity nature of the samples. Therefore, from the current study, we attempt to dope cobalt in Zinc oxide by varying weight percentages and to study the conductivity properties.

2. Experimental

2.1. Preparation of the pure and Co doped ZnO nanoparticles

The following high purity chemicals such as zinc acetate dehydrate (Zn $(CH_3COO)_2{\cdot}2H_2O$), cobalt acetate tetrahydrate (Co $(CH_3COO)_2{\cdot}4H_2O$), sodium hydroxide (NaOH), ethanol and methanol (99.998%) were used as the precursors without further purification. For the preparation of pure ZnO nanoparticles (NPs), specific amounts of zinc acetate and NaOH are dissolved in 50 ml methanol which is added drop wise and then stirred with heating at 325 K for 2 h. The precipitate is separated from the solution by filtration, washed several times with distilled water and ethanol then dried in air at 400 K to obtain ZnO nanocrystals. The samples obtained were annealed at 673 K for 8 h. For the synthesis cobalt doped ZnO, zinc acetate dehydrate and cobalt acetate dehydrate were dissolved in methanol (100 ml) and other containing of NaOH in methanol (100 ml) were prepared and added by constant magnetic stirring while heating at 325 K for 2 h. Precipitate is then separated from the solution by filtration, washed several times with distilled water and ethanol then dried in air at 400 K to obtain Co doped ZnO nanoparticles and annealing at 673 K for 8 h.

2.2. Characterization of samples

For electrical conductivity measurements, the powder samples were pressed uniaxially into a pellet of thickness 4–5 mm and of diameter 10 mm by applying pressure of 120 Mpa for 3 min. Pellets were sintered at 573 K for 3 h for thermal stabilization. Fine quality silver paint was applied on both sides of the pellets for good electrical contacts. The DC electrical conductivity measurements were carried by two probe method in the temperature range 300–650 K. The samples were analyzed by the following characterization studies. The samples were analyzed by the following characterization studies done using x-Ray powder diffraction (XRD) (XPERT-PRO (Model: PW-3710) operated at 45 kV and 40 mA with a Cu-K_α radiation source of wavelength 1.5406 Å), scanning electron microscope (SEM) (Model: JSM6100), transmission electron microscope (TEM: Hitachi-Model: H-7500) and DC electrical conductivity measurements using KEITHLEY source meter (model 2400).

2.3. Different relations used for measurement of properties

The lattice constants of pure and Co doped ZnO nanocrystals were determined using following formula

$$\sin^2\theta = \frac{\lambda^2}{4a^2}\left[\frac{4}{3}(h^2+hk+k^2)+\frac{a^2l^2}{c^2}\right] \quad (1)$$

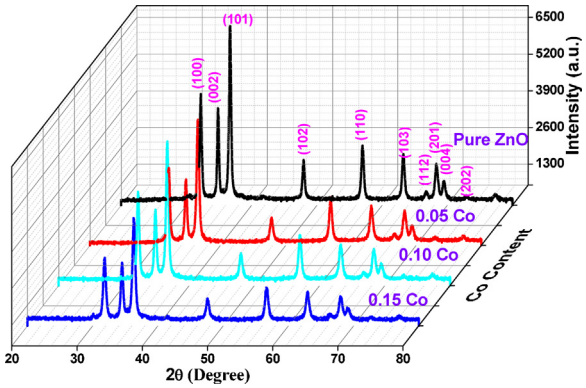

Fig. 1. X-ray diffraction patterns of $Zn_{1-x}Co_xO$ nanoparticles.

where 'θ' is the angle of diffraction, 'λ' is wavelength, 'a' & 'c' are lattice constants and h, k and l are miller indices. Considering the first order approximation (n = 1) for the (100) plane, the lattice constant 'a' is obtained through the relation

$$a = \frac{\lambda}{\sqrt{3}\sin\theta} \quad (2)$$

Lattice constant 'c' is derived for the plane (002) by the relation

$$c = \frac{\lambda}{\sin\theta} \quad (3)$$

The volume of unit cell can be calculated using equation,

$$V = 0.866 \times a^2 \times c \quad (4)$$

The parameter 'u' can be calculated by the formula doping-induced effect of bond length ZnO is analyzed.

$$u = \frac{a^2}{3c^2} + 0.25 \quad (5)$$

Average crystallite sizes were estimated using Debye–Scherrer's equation

$$D = \frac{K\lambda}{\beta\cos\theta} \quad (6)$$

Strain induced broadening (ε) is given by the Wilson formula:

$$\varepsilon = \frac{\beta_{hkl}}{4\tan\theta} \quad (7)$$

where 'ε' is the root mean square value of the micro strain. The readings were recorded during slow cooling after heating cycle and the electrical conductivity (σ) was calculated by the formula:

$$\sigma = \left(\frac{\mathrm{I}\times\mathrm{t}}{\mathrm{V}\times\mathrm{A}}\right) \quad (8)$$

where 'V' is the applied voltage, 'I' is the measured current; 'A' is the area of the pellet and 't' the thickness of the pellet.

3. Results and discussions

3.1. X-ray diffraction study

Fig. 1 shows x-ray diffraction patterns (XRD) of pure and Co doped ZnO nanoparticles. The XRD peaks are located at angle (2θ) corresponds to (100), (002), (101), (102), (110), (103), (112), (201) and (004) planes attributed to ZnO. The XRD peaks show the hexagonal (wurtzite) crystal structure of all prepared samples. In reported literatures the spinel Co_3O_4 peaks are observed as a secondary phase even for the lowest dopant concentration x = 0.1 at sufficiently high calcination temperature of 600 °C [23,24]. Fig. 1 confirms no extra or any impurity phases evident in Co doped ZnO

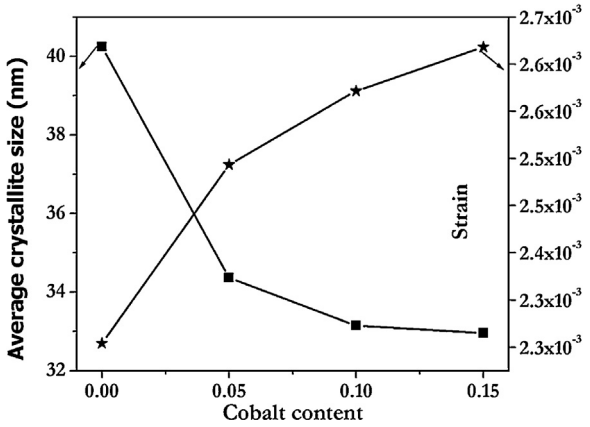

Fig. 2. Average crystallite size and strain Vs Co content of Zn1-xCoxO nanoparticles.

samples, indicates that the prepared samples are single in phase thereby clearly indicating that cobalt has been incorporated in to the lattice as a substitutional atom. Lowering intensity and increase in full width half maxima (FWHM) in the results of XRD is also observed due to the effect of cobalt incorporation in zinc oxide. A small shift is also observed in the peaks for the cobalt doped ZnO samples due to replacement of cobalt Co^{2+} with Zn^{2+} evident as decrease of intensity peak (101) as shown in Fig. 1. Evidence of peak reduction in terms of peak intensity can influence particle size or lattice strain. Fig. 2 shows the variation for average crystallite size and strain for cobalt concentration for $Zn_{1-x}Co_xO$ nanoparticles. The changes produced in strain are sufficient to produce the formation of clusters or precipitation which could further evident using transmission electron microscope (TEM) and scanning electron microscope (SEM).

No secondary phases or existence of Co^{3+} ions in our samples is evident in XRD studies, suggests that the Co^{2+} ions are responsible for the deformation of the lattice structure when they are substituted for Zn^{2+} ions in ZnO. Deformation variation is observed on basis of increase in lattice parameters (a,c) and volume as evident in Table 1. Smaller variation observed is attributed to mismatch in radius of cobalt and zinc oxide, in octahedral environment. The lattice parameters is expected to increase due to cobalt doing as assuming tetrahedral environment with high spin state for $Co^{(2+)}$ (0.745 Å) and low spin state for $Co^{(2+)}$ (0.65 Å) are smaller than $Zn^{(2+)}$(0.60Å) as reported elsewhere [25]. The increase in volume resulted a change in oxygen parameter, which increases with increase in cobalt. These increases in defect density which can cause a change in the lattice parameters of ZnO, also results in the non-linear behavior of electrical conductivity.

3.2. Morphological study

3.2.1. Transmission electron microscope (TEM) study

Fig. 3 reveals the homogeneous distribution of Co^{2+} particles in the ZnO lattice along with particle sizes. Fig. 3(a) shows the ZnO nanoparticles are hexagonal in shape with average particles size around 30 nm. Fig. 3(b) and (c) shows the TEM images for Co–ZnO samples, suggests that the particles are spherical in shape with average particles size is around ~20 nm and these results correlate with our XRD results. Average particle size of Co–ZnO nanoparticles reduces when compared of pure ZnO, showing small grain growth of doped samples.

3.2.2. Scanning electron microscope(SEM) study

Fig. 4 shows scanning electron microscope (SEM) images for pure and Co–ZnO nanoparticles. Surface morphology shows uniform evenly distributed grains with hexagonal structure in the samples, as shown in Fig. 4. SEM micrographs also reveal that cobalt doped ZnO nanoparticles decreases in average grain size which can also evident from our XRD measurements and TEM. This decrease in average grain size with increasing doping concentration was also reported by Vijayaprasath et al. [26] in Co-doped Ni/ZnO nanoparticles.

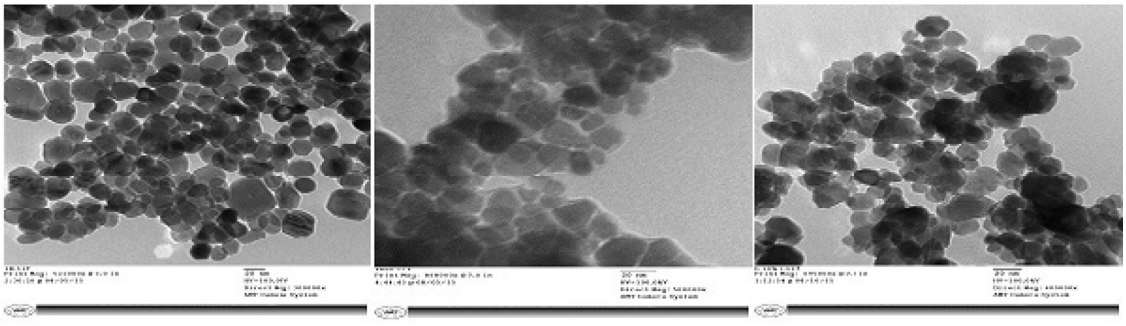

Fig. 3. TEM image of (a) ZnO (b) $Zn_{0.95}Co_{0.05}O$ and (c) $Zn_{0.85}Co_{0.15}O$.

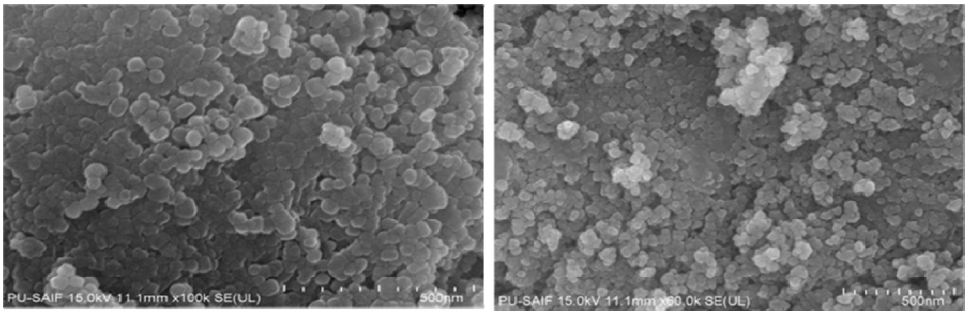

Fig. 4. SEM image of (a) ZnO and (b) $Zn_{0.95}Co_{0.05}O$.

Table 1
Structural parameters, average crystallite size and strain of $Zn_{1-x}Co_xO$ nanoparticles.

Samples (% Co)	Lattice parameters (Å)		Volume (Å)	c/a ratio	u (distortion parameter)	Bond length (Å)
	a	c				
X = 0	3.2087	5.1475	45.8953	1.6042	0.3795	1.9536
X = 0.05	3.2222	5.1642	46.4325	1.6027	0.3797	1.9612
X = 0.10	3.2262	5.1658	46.5616	1.6012	0.3800	1.9630
X = 0.15	3.2435	5.1969	47.3469	1.6022	0.3798	1.9740

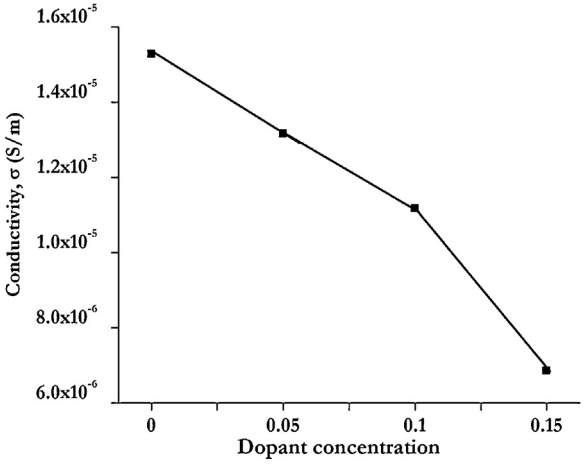

Fig. 5. Variation of conductivity, σ (S/m) with dopant concentration.

3.3. Electrical conductivity

Decrease in conductivity with increase in doping concentration of cobalt in ZnO is shown in Fig. 5. This is consistent with the literature and is also evident from SEM analysis [27,28] which is attributed to the increased defect scattering due to the addition of Co^{2+} ions. Free electrons from the donor levels are trapped by the divalent ions, results in the decrease in the n-type donor carrier concentration and increase in resistivity. The small amount of cobalt within soluble limit depresses the carrier concentration making the ZnO higher resistive [29]. Critical nature of resistivity evident in the magnetic based semiconductors was attributed to distribution of carriers through exchange interaction [30].

Fig. 6 shows the observed values of conductivity which rises slowly with increase of temperature above 470 K for increase in cobalt doping concentration. At a temperature higher than 450 K, as shown in Fig. 6(a) ln(conductivity) is plotted against the inverse of temperature. Similarly at a temperature lower than 450 K. Fig. 6(b) show ln(conductivity) plotted against the inverse of temperature elucidating a non-linear behavior compatible with the ionic radius of Co^{2+} ions to that of Zn^{2+} ions. Substitution of Co^{2+} ions in Zn^{2+} lattice site is expected to create certain oxygen vacancies or zinc interstitials. These vacancies can perform as donors as well as deform the lattice structure to maintain the charge neutrality. The variation in conductivity is also dependent on thermal energy and below Curie temperatures. Conductivity is largely dependent on charge carrier mobility which can be observed in Fig. 6(a) and (b).

To understand the conductivity mechanism in cobalt doped zinc oxide, the conductivity curve shown is divided in to two different regions (I, II). The linear region I (high temperature region) refers to linear conduction mechanism and region II is transition region (low temperature region). For these regions, the electrical conductivity of $Zn_{(1-x)}Co_xO$ can be analyzed by the Arrhenius equation which relates the electrical conductivity and the temperature is given by

$$\sigma = \sigma_0 \exp\left(\frac{-E_a}{k_B T}\right) \quad (9)$$

where σ_0 is the pre-exponential factor and E is the activation energy for the conductivity. E_a values for region II were respectively calculated from the linear portions of Fig. 6(a) and the E_a values of region I are calculated from the slope of the Arrhenius plot as shown in Fig. 6(b). Since, there are two slopes two conduction mechanisms are possible, observed two-stage temperature dependence of conductance (σ) may be represented as:

$$\sigma = \sigma_L \exp\left(\frac{-E_{aL}}{k_B T}\right) + \sigma_H \exp\left(\frac{-E_{aH}}{k_B T}\right) \quad (10)$$

In above equation, σ_L and σ_H are pre-exponential factors, Ea_L and Ea_H are the activation energy for low and high temperature conductance stages respectively. As shown in Fig. 7 Arrhenius plots of $Zn_{1-x}Co_xO$ were used to calculate activation energies and are given in Table 2 for different values E_a in region I (in high temperature range 473–508 K) and Ea in region II (in low temperature range 363–473 K).

The measured activation energies for two regions suggest the operating mechanisms of trapped or scattering ions. As the doping concentration increases, the activation energy is raised which would account for the raise in atomic defects and are electrically

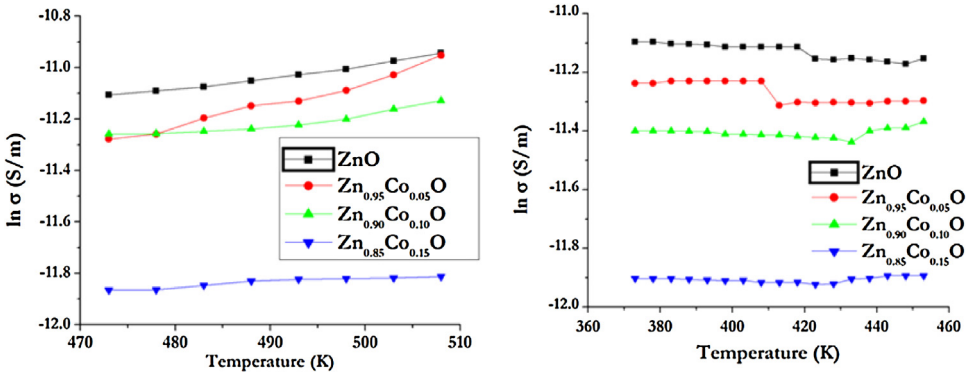

Fig. 6. Variation of electrical conductivity with temperature in two different regions (a) 473–508 K and (b) 360–460 K.

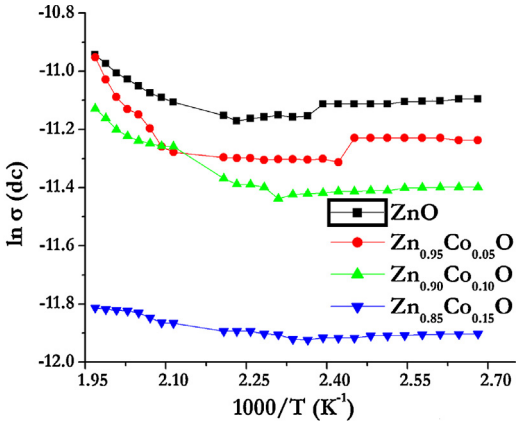

Fig. 7. Arrhenius plot of dc conductivity with variation of temperature.

Table 2
Activation energy values of different doping concentrations of cobalt.

Cobalt concentration	Ea (eV) region II (low temperature range: 363–473 K)	Ea (eV) region I (high temperature range: 473–508 K)
X = 0	1.08082	0.179582
X = 0.05	0.99768	0.284339
X = 0.10	0.93548	0.395746
X = 0.15	0.91454	0.433159

active at the grain boundary. Hence, when the cobalt is doped, both the potential barrier height and activation energy are raised to the formation of barrier at the grain–grain interface. E_{aL} with values of 1.08–0.91 meV for region I at low temperature region (363–453 K) vary and E_{aH} with values of 0.17–0.43 eV for region II at high temperature region (473–508 K) respectively. The values of activation energies suggest the shallow nature with deep donor levels along with impurity level in band gap of Cobalt doped ZnO.

Thermal excitation of electrons from donor levels to the conduction band takes place for increase in temperature. Thermal activations in region I is due to deep donor level ions contributing to the conduction band. With increase in doping of cobalt in ZnO for temperature range (363–473 K), the values of activation energy (E_{aL}) are decreasing due to donor carrier density which brings the Fermi level up in the band gap. At low temperature, for a doped semiconductor most of the free electrons are recaptured by donors itself. The electrons then do not have adequate energy to jump from donor levels to conduction band. By hopping from one level to another in the impurity band they conduct, making the free electron band conduction less important [16]. Thus, the free electron band conduction is no more a dominating conduction mechanism in the low temperature range. Low temperature activation energy of ZnO samples is possibly associated with one of the following two donor ionization processes:

$$V_o + V^+{}_o + e^-$$

proposed by Simpson and Cordero [31] for oxygen vacancy (V_o) or the zinc interstitials:

$$Zn + i \rightarrow Zn^+ + I + e^-$$

The reversal takes place for high temperature range (473–508 K), where cobalt ions creates wide energy levels for ZnO resulting in compensation for donor carrier density increasing activation energy values. The high temperature activation energy can be associated with desorption of $O_2{}^-$ species [32] according to the equation, $O^-{}_2 + O_2 + e^-$

Here, region II corresponds to a transition region, in which more charge carriers are ionized from the shallow donor level and then, in turn, the depletion of charge carriers takes place. With increase in temperature, more charge carriers overcome the activation energy barrier and these carriers participate in the electrical conduction. Due to the higher ionization potential of the substituted Co atoms which cannot be easily ionized like Zn atoms, thus the donor concentration being lowered by the addition of Co and this results in decrease in electrical conductivity. From DC conductivity studies, the potential barrier, donor concentration, point defects and adsorption–desorption of oxygen are believed to be controlling the conductivity of ZnO and Cobalt doped ceramic system.

4. Conclusions

Co doped ZnO nanoparticles were synthesized through co-precipitation method and annealed at 673 K for 8 h. The X-ray diffraction study confirmed that the synthesized ZnO nanoparticles with hexagonal (wurtzite) crystal structure. Cobalt doping in ZnO showed reduction in intensity for peak (101) at 36°. Microstructures of the nanoparticles have been examined by TEM and evaluation of average particle size was in the range of 20 nm. SEM images of nanoparticles show the uniform shape with decreasing grain size for samples of $Zn_{(1-x)}Co_xO$ samples. A non-linear decrease in electrical conductivity is observed with increasing temperature among the samples. Temperature-dependent electrical conductivity confirms the semiconducting nature of these $Zn_{(1-x)}Co_xO$ samples.

References

[1] C. Klingshirn, Phys. Status Solidi B, 244, 3027–3073 (2007).
[2] E. Wong and P. Searson, Appl. Phys. Lett., 74, 2939 (1999).
[3] S. Choopun, R. Vispute, W. Noch, A. Balsamo, R. Sharma, T. Venkatesan, A. Iliadis and D. Look, Appl. Phys. Lett., 75, 3947–3949 (1999).
[4] X.D. Wang, J. Zhou, J.H. Song, J. Liu, N. Xu and Z.L. Wang, Nano Lett., 6, 2768–2772 (2006).
[5] P.D. Yang, H.Q. Yan, S. Mao, R. Russo, J. Johnson, R. Saykally, N. Morris, J. Pham, R. He and H.J. Choi, Adv. Funct. Mater., 12, 323–331 (2002).
[6] M. Law, L.E. Greene, J.C. Johnson, R. Saykally and P.D. Yang, Nat. Mater., 4, 455–459 (2005).
[7] S.C. Navale, S.W. Gosavi and I.S. Mulla, Talanta, 75, 1315–1319 (2008).
[8] Jun Zhang, Shurong Wang, Yan Wang, Mijuan Xu, Huijuan Xia, Shoumin Zhang, Weiping Huang, Xianzhi Guo and Shihua Wu, Sens. Actuators B, 139, 411–417 (2009).
[9] D.C. Look, B.C. Ya, I. Alivov and S.J. Park, Phys. Status Solid A, 2203–2212 (2004).
[10] S.J. Pearton, D.P. Norton, K. Ip, Y.W. Heo and T. Steiner, Prog. Mater. Sci., 50, 293–340 (2005).
[11] W. Liang, B.D. Yuhas and P. Yang, Nano Lett., 9, 892–896 (2009).
[12] K.M. Whitaker, M. Raskin, G. Kiliani, K. Beha, S.T. Ochsenbein, N. Janssen, M. Fonin, U. R∈udiger, A. Leitenstorfer, D.R. Gamelin and R. Bratschitsch, Nano Lett., 11, 3355–3360 (2011).
[13] H. Woo, C. Kwak, J. Chung and J. Lee, ACS Appl. Mater. Interfaces, 6, 22553–22560 (2014).
[14] H.B. Carvalho, M.P.F. Godoy, R.W.D. Paes, M. Mir, F. A.O.Zevallos, M.J.S.P. Iikawa, V.A. Brasil, W.B. Chitta, M.A. Ferraz, A.C.S. Boselli and J. Sabioni, Appl. Phys., 108, 033914–033919 (2010).
[15] Y.Z. Yoo, T. Fukumura, Z. Jin et al., J. Appl. Phys., 90, 4246 (2001).
[16] R. Kumar and N. Khare, Thin Solid Films, 516, 1302–1307 (2008).
[17] T.K. Roy, D. Sanyal, D. Bhowmick and A. Chakrabarti, Mater. Sci. Semicond. Process., 16, 332–336 (2013).
[18] L. Yan, C. Ong and X. Rao, J. Appl. Phys., 96, 508–511 (2004).
[19] D. Shankar Birajdar, P. Pankaj Khirade, S. Tukaram Saraf, R.C. Alange and K.M. Jadhav, J. Alloys Compd., 691, 355–363 (2017).
[20] Arockia Jayalatha Kulandaisamy, Chitra Karthek, Prabakaran Shankar, Ganesh Kumar Mani and John Bosco Balaguru Rayappan, Ceram. Int., 42, 1408–1415 (2016).
[21] J.M.D. Coey, Kwanruthai Wongsaprom, J. Alaria and M. Venkatesan, J. Phys. D: Appl. Phys., 41, 134012 (2008).
[22] Y. Caglar, J. Alloy Compd., 560, 181–188 (2013).
[23] S.K. Mandal, A.K. Das and T.K. Nath, J. Appl. Phys., 100, 104315 (2006).
[24] V.K. Sharma, M. Najim, A.K. Srivastava and G.D. Varma, JMMM, 324, 683–689 (2012).
[25] O.D. Jayakumar, I.K. Gopalakrishnan and S.K. Kulshreshtha, J. Mater. Chem., 15, 3514 (2005).

[26] G. Vijayaprasath, R. Murugan, S. Asaithambi, G. Anandha Babu, P. Sakthivel, T. Mahalingam, Y. Hayakawa and G. Ravi, Appl. Phys. A, 122, (122) (2016).
[27] C. Fitzgerald, M. Venkatesan, J. Lunney, L. Dorneles and J. Coey, Appl. Surf. Sci., 24, 493–496 (2005).
[28] R.B. Kale and C.D. Lokhande, Mater. Res. Bull., 39, 1829–1839 (2004).
[29] J. Han, P.Q. Mantas and A.M.R. Senos, J. Eur Ceram. Soc., 22, 49–59 (2002).
[30] F. Matsukura, H. Ohno, A. Shen and Y. Sugawara, Phys. Rev. B, 57, R2037 (1998).
[31] J.C. Simpson and J.F. Cordero, J. Appl. Phys., 63, 1988 (1781).
[32] Satoru Fujitsu, Kunihito Koumoto, Hiroaki Yanagida, Yuichi Watanabe and Hiroshi Kawazoe, J. Appl. Phys., 38, 1534–1538 (1999).